Linear theory of a dielectric-loaded rectangular Cerenkov maser with a sheet electron beam*

Chen Ye (陈 晔)[a)b)†], Zhao Ding(赵 鼎)[b)], Liu Wen-Xin(刘文鑫)[b)], Wang Yong(王 勇)[b)], and Wan Xiao-Sheng(万晓声)[a)b)]

[a)] *Key Laboratory of High Power Microwave Sources and Technologies, Institute of Electronics, Chinese Academy of Sciences, Beijing* 100190, *China*

[b)] *Graduate University of Chinese Academy of Sciences, Beijing* 100049, *China*

(Received 6 January 2012; revised manuscript received 9 April 2012)

A three-dimensional model of a dielectric-loaded rectangular Cerenkov maser with a sheet electron beam for the beam-wave interaction is proposed. Based on this model, the hybrid-mode dispersion equation is derived with the Borgnis potential function by using the field-matching method. Its approximate solution is obtained under the assumption of a dilute electron beam. By using the Ansoft high frequency structural simulator (HFSS) code, the electromagnetic field distribution in the interaction structure is given. Through numerical calculations, the effects of beam thickness, beam and dielectric-layer gap distance, beam voltage, and current density on the resonant growth rate are analysed in detail.

Keywords: rectangular Cerenkov maser, beam-wave interaction, hybrid-mode, dispersion equation, Borgnis potential function

PACS: 41.60.Bq, 94.20.wj **DOI:** 10.1088/1674-1056/21/10/104103

1. Introduction

Research on Cerenkov masers dates from the late 1940s. Since then, a series of far-reaching achievements has been made. As a novel type of high power microwave source, the Cerenkov maser is well known for its high power and high frequency coherent radiation and a wide tunable working frequency range, which shows promising prospects in radar, communication systems, plasma heating, material sciences, and so on.[1−10]

As one of the most essential members of the Cerenkov maser family, the rectangular Cerenkov maser (RCM) is characterized by the beam-wave interaction between the electromagnetic fields in a planar slow-wave structure and a sheet electron beam. Compared with the cylindrical Cerenkov maser, the focusing of the beam in the RCM can be realized by using periodic permanent magnets because of the smaller space-charge force in the sheet beam. In the RCM, the total beam current can be enhanced by enlarging the beam size instead of increasing the beam current density which can lead to reduced interaction efficiency and less stable beam confinement. Usually, the RCM adopts dielectric-loaded or metal-grating slow-wave structure as its interaction structure. In contrast to the metal-grating RCM, the arc discharge problem caused by the high current density can be avoided in the dielectric-loaded RCM. Meanwhile, the RCM can operate in an ultra-broad frequency band that is able to reach the one-octave level when a thick enough dielectric liner is used.[11] However, sometimes dielectric breakdown problem occurs if the device works in a state of high current density, which will eventually result in the pulse shortening in operation.

Significant experimental work on the dielectric-loaded RCM has been performed since the 1980s. The output power is at the 100-kW level for oscillators and 10-MW level with a pulse of 100 ns for amplifiers. In 1988, Walsh *et al.*[12] first did the dielectric-loaded Cerenkov maser work in the far-infrared frequency band. In 1990, Garate *et al.*[13] obtained a growth rate of 11 dB over the interaction length of 21 cm for the X-band dielectric-loaded Cerenkov maser. Subsequently, in the early 2000s, Calsten[14] put forward a conceptual design of the RCM that was applied in a low-frequency communication system, and according to the PIC simulation, he obtained 1.2-dB/cm gain at 28.7 GHz using the sheet electron beam (140 kV,

*Project supported by the National Natural Science Foundation of China (Grant Nos. 60801031 and 10905032) and the Knowledge Innovation Project of the Chinese Academy of Sciences (Grant No. YYYJ-1123-5).

†Corresponding author. E-mail: chenye07@mails.gucas.ac.cn

© 2012 Chinese Physical Society and IOP Publishing Ltd

15 A), and an interaction efficiency of about 15%–25%.

In the present paper, a three-dimensional beam-wave interaction theory in the dielectric-loaded RCM is established. The dispersion equation in the RCM is derived by solving an equivalent multilayer field problem for the sheet beam linearly interacting with the hybrid modes. Its approximate solution can be obtained under a low current density limit. Numerical results show the influences of the principal structural and electrical parameters on the resonant growth rate, which will be a useful reference for designing the RCM.

2. Model and formula

Figure 1 shows a three-dimensional (3D) model of the dielectric-loaded RCM with a relativistic sheet electron beam, which consists of a rectangular waveguide of height b and width a with double dielectric layers. d_1 and d_2 are defined as the thickness of the top and bottom dielectric layers, respectively. A sheet electron beam interacts with the guided waves in the structure, and the beam is immersed in a strong axial magnetic field that constrains electron motion only along the z axis. The drift velocity of the beam v_0 is constant, and t denotes the beam thickness. All the derivations in this paper are based on this model.

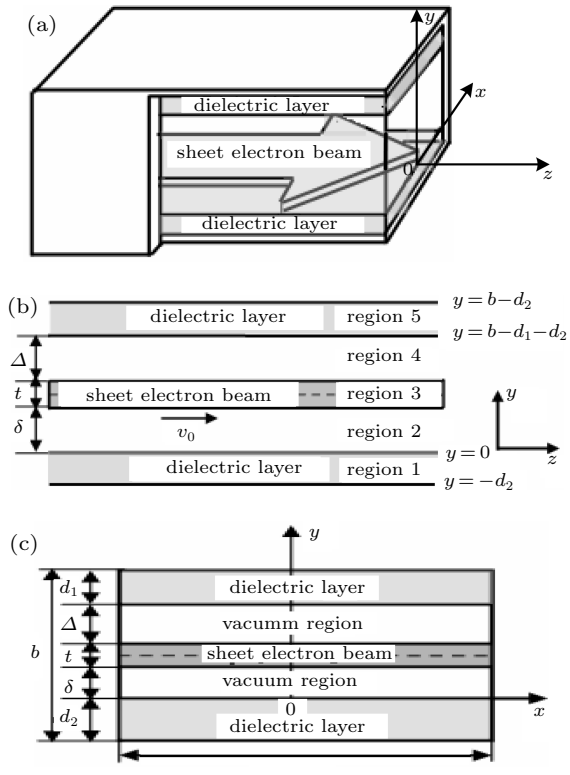


Fig. 1. Model of the dielectric-loaded RCM. (a) 3D model, (b) longitudinal section view, (c) tansverse section view.

Choosing the z axis as the longitudinal direction, the electromagnetic mode in this structure is a hybrid mode that simultaneously includes the z axial field components, E_z and H_z, which can be represented by the superposition of the normal TE and TM modes in a perfect metal waveguide. However, the hybrid mode discussed here can be simply expressed as a transverse magnetic mode along the y direction, TM_{ylq}, where l is defined as the x-direction wave-number and q is defined as the mode sequence number.[15] For a self-consistent analysis, the electron motion equations and Maxwell equations must be combined to obtain a solution. As shown in Fig. 1, the whole structure is divided into five regions. Regions 1, 2, 3, 4, and 5 are defined as the regions $-d_2 < y < 0$, $0 < y < \delta$, $\delta < y < \delta + t$, $\delta + t < y < b - d_1 - d_2$, and $b - d_1 - d_2 < y < b - d_2$, respectively.

By linearizing Lorentz-force equations and Maxwell equations, beam region 3 can be replaced by the equivalent dielectric layer with an effective permittivity constant as follows:[16,17]

$$\overrightarrow{\overrightarrow{\varepsilon}} = \begin{pmatrix} 1 & 0 & 0 \\ 0 & 1 & 0 \\ 0 & 0 & 1+\chi_b \end{pmatrix}, \tag{1}$$

where $\chi_b = -\omega_{\mathrm{p}}^2/\{\gamma^3(\omega - v_0\beta)^2\}$ reflects the electron polarization response to the perturbing field component E_z. $\omega_{\mathrm{p}} = \sqrt{(e^2 n_0)/(\gamma m_0 \varepsilon_0)}$ represents the plasma frequency, e, n_0, m_0, β, γ, and v_0 denote one charge electric quality, electron density, electron rest mass, propagation constant, relativistic factor, and drift velocity of the beam, respectively. Hence the field solution can be reduced to an equivalent multilayer field problem.

Based on the above analysis, the Borgnis potential function U can be expressed by using the method of variable separation as

$$U_{yi} = (A_i^+ \mathrm{e}^{\mathrm{j}k_i y} + A_i^- \mathrm{e}^{-\mathrm{j}k_i y}) \times \sin\left[k_x\left(x + \frac{a}{2}\right)\right] \mathrm{e}^{-\mathrm{j}\omega t + j\beta z}, \tag{2}$$

where k_i (i = 1–5) represent the y direction propagation constants in regions 1, 2, 3, 4, and 5, respectively; A_i^+ and A_i^- (i = 1–5) separately denote the forward and backward amplitude constants; k_x is defined as the x-direction propagation constant; β denotes the z-direction propagation constant; other parameters can be written as

$$k_1 = k_d,\ k_2 = -\mathrm{j}k_0,\ k_3 = -\mathrm{j}k_b,\ k_4 = -\mathrm{j}k_0,\ k_5 = k_d,$$

$$k_b = \sqrt{k_x^2 + \beta^2 - \left(\frac{\omega}{c}\right)^2}\sqrt{\frac{k_x^2 + \Theta\beta^2}{k_x^2 + \beta^2}},$$

$$k_d = \sqrt{\left(\frac{\omega}{c}\right)^2 \varepsilon_r - k_x^2 - \beta^2},$$

$$k_0 = \sqrt{k_x^2 + \beta^2 - \left(\frac{\omega}{c}\right)^2},\ k_x = \frac{l\pi}{a},\ l = 1, 2, \ldots,$$

$$\Theta = \begin{cases} 1 + \chi_b, & \text{in the region 3,} \\ 1, & \text{in other regions,} \end{cases}$$

$$\chi_b = \frac{-\omega_{\rm p}^2}{\gamma^3(\omega - \nu_0\beta)^2},$$

where k_d, k_0, and Θ being the intermediate variables, and ε_r representing the relativistic dielectric constant.

According to the corresponding relations between the Borgnis potential function and the electromagnetic field components, E_z and H_x can be expressed as

$$E_{zi} = \frac{{\rm j}\beta}{k_x^2 + \Theta\beta^2}\frac{\partial U_{yi}}{\partial y}, \tag{3}$$

and

$$H_{xi} = \frac{-\omega\varepsilon\Theta\beta}{k_x^2 + \Theta\beta^2}U_{yi}. \tag{4}$$

Hence, the electromagnetic field components in regions 1, 2, 3, 4, and 5 can be expressed as

$$E_{z1} = \frac{-\beta k_d}{k_x^2 + \beta^2}(A_1^+ {\rm e}^{{\rm j}k_d y} - A_1^- {\rm e}^{-{\rm j}k_d y}) \sin\left[k_x\left(x + \frac{a}{2}\right)\right] {\rm e}^{-{\rm j}\omega t + {\rm j}\beta z}, \tag{5a}$$

$$E_{z2} = \frac{{\rm j}\beta k_0}{k_x^2 + \beta^2}(A_2^+ {\rm e}^{k_0 y} - A_2^- {\rm e}^{-k_0 y}) \sin\left[k_x\left(x + \frac{a}{2}\right)\right] {\rm e}^{-{\rm j}\omega t + {\rm j}\beta z}, \tag{5b}$$

$$E_{z3} = \frac{{\rm j}\beta k_b}{k_x^2 + (1+\chi_b)\beta^2}(A_3^+ {\rm e}^{k_b y} - A_3^- {\rm e}^{-k_b y}) \sin\left[k_x\left(x + \frac{a}{2}\right)\right] {\rm e}^{-{\rm j}\omega t + {\rm j}\beta z}, \tag{5c}$$

$$E_{z4} = \frac{{\rm j}\beta k_0}{k_x^2 + \beta^2}(A_4^+ {\rm e}^{k_0 y} - A_4^- {\rm e}^{-k_0 y}) \sin\left[k_x\left(x + \frac{a}{2}\right)\right] {\rm e}^{-{\rm j}\omega t + {\rm j}\beta z}, \tag{5d}$$

$$E_{z5} = \frac{-\beta k_d}{k_x^2 + \beta^2}(A_5^+ {\rm e}^{{\rm j}k_d y} - A_5^- {\rm e}^{-{\rm j}k_d y}) \sin\left[k_x\left(x + \frac{a}{2}\right)\right] {\rm e}^{-{\rm j}\omega t + {\rm j}\beta z}, \tag{5e}$$

$$H_{x1} = \frac{-\omega\varepsilon_0\varepsilon_r\beta}{k_x^2 + \beta^2}(A_1^+ {\rm e}^{{\rm j}k_d y} + A_1^- {\rm e}^{-{\rm j}k_d y}) \sin\left[k_x\left(x + \frac{a}{2}\right)\right] {\rm e}^{-{\rm j}\omega t + {\rm j}\beta z}, \tag{6a}$$

$$H_{x2} = \frac{-\omega\varepsilon_0\beta}{k_x^2 + \beta^2}(A_2^+ {\rm e}^{k_0 y} + A_2^- {\rm e}^{-k_0 y}) \sin\left[k_x\left(x + \frac{a}{2}\right)\right] {\rm e}^{-{\rm j}\omega t + {\rm j}\beta z}, \tag{6b}$$

$$H_{x3} = \frac{-\omega\varepsilon_0(1+\chi_b)\beta}{k_x^2 + (1+\chi_b)\beta^2}(A_3^+ {\rm e}^{k_b y} + A_3^- {\rm e}^{-k_b y}) \sin\left[k_x\left(x + \frac{a}{2}\right)\right] {\rm e}^{-{\rm j}\omega t + {\rm j}\beta z}, \tag{6c}$$

$$H_{x4} = \frac{-\omega\varepsilon_0\beta}{k_x^2 + \beta^2}(A_4^+ {\rm e}^{k_0 y} + A_4^- {\rm e}^{-k_0 y}) \sin\left[k_x\left(x + \frac{a}{2}\right)\right] {\rm e}^{-{\rm j}\omega t + {\rm j}\beta z}, \tag{6d}$$

$$H_{x5} = \frac{-\omega\varepsilon_0\varepsilon_r\beta}{k_x^2 + \beta^2}(A_5^+ {\rm e}^{{\rm j}k_d y} + A_5^- {\rm e}^{-{\rm j}k_d y}) \sin\left[k_x\left(x + \frac{a}{2}\right)\right] {\rm e}^{-{\rm j}\omega t + {\rm j}\beta z}. \tag{6e}$$

By applying the boundary conditions of the tangent electric field components in the planes $y = -d_2$ and $y = b - d_2$, and the continuous conditions of the tangent field components, the hybrid-mode dispersion equation can be derived through complicated algebraic operations as

$$\begin{aligned} D(\omega, k_z, \chi_b) = {} & \frac{k_b(\Psi_1 + 1) + \Theta k_0(\Psi_1 - 1)}{k_b(\Psi_1 + 1) - \Theta k_0(\Psi_1 - 1)} \\ & - \frac{k_b(\Psi_2 + 1) + \Theta k_0(\Psi_2 - 1)}{k_b(\Psi_2 + 1) - \Theta k_0(\Psi_2 - 1)} {\rm e}^{-2k_b t} \\ = {} & 0, \end{aligned} \tag{7}$$

where

$$\Psi_1 = \frac{\varepsilon_r k_0 - k_d \tan(k_d d_2)}{\varepsilon_r k_0 + k_d \tan(k_d d_2)} {\rm e}^{2k_0\delta},$$

$$\Psi_2 = \frac{\varepsilon_r k_0 - k_d \tan(k_d d_1)}{\varepsilon_r k_0 + k_d \tan(k_d d_1)} {\rm e}^{2k_0\Delta},$$

The analytic solution of Eq. (7), i.e., the complex propagation constant when the working frequency is kept unchanged, can be obtained by solving the transcendental equation numerically. However, under the assumption of a dilute electron beam, an approximate solution can be easily obtained. In the dielectric-loaded RCM, there exist the guided surface-wave and the space-charge wave simultaneously. According to the coupling mode theory, the coupling between the two waves becomes strong when their phase velocities are close to each other,[18] which is commonly known as the synchronous condition. The coupled fields are hence modified from the fields of an uncoupled guided surface-wave. Since the beam is dilute (i.e. $\chi_b \ll 1$), the field modification due to the coupling is moderate. Based on this point, Eq. (7) is expanded around $\chi_b = 0$ and the resonant point ($\omega_{\rm res}$, $\beta_{\rm res}$) by using the Taylor series, as follows:

$$D(\omega,\beta,\chi_b) = D(\omega,\beta,\chi_b)\big|_{(\omega_{\rm res},\beta_{\rm res},\chi_b=0)} + \delta\beta\frac{\partial D(\chi_b=0)}{\partial\beta}\Big|_{(\omega_{\rm res},\beta_{\rm res})} + \chi_b\frac{\partial D}{\partial\chi_b}\Big|_{(\omega_{\rm res},\beta_{\rm res},\chi_b=0)}. \quad (8)$$

Through algebraic operations, the resonant growth rate (i.e., the imaginary part of $\delta\beta$) is obtained as

$$\delta\beta = \left[\frac{(\omega_{\rm p}/\gamma)^2\dfrac{1}{v_o^2}\dfrac{\partial D(\beta,\chi_b)}{\partial\chi_b}}{\dfrac{\partial D(\beta,\chi_b)}{\partial\beta}}\right]^{1/3}, \quad (9)$$

where

$$\frac{\partial D(\beta_{\rm res},\chi_b)}{\partial\chi_b}\bigg|_{\chi_b=0} = \frac{F\dfrac{\partial E}{\partial\chi_b}-E\dfrac{\partial F}{\partial\chi_b}}{F^2} - \frac{H\frac{\partial G}{\partial\chi_b}-G\dfrac{\partial H}{\partial\chi_b}}{H^2}\,{\rm e}^{-2k_0t} + \sqrt{k_x^2+\beta^2-\left(\frac{\omega}{c}\right)^2}\,\frac{\beta^2 t\,{\rm e}^{-2k_0t}}{k_x^2+\beta^2}\,\frac{G}{H},$$

$$\frac{\partial D(\beta_{\rm res},\chi_b=0)}{\partial\beta} = \frac{\partial\Psi_1}{\partial\beta} - \frac{\partial\Psi_2}{\partial\beta}\,{\rm e}^{-2k_0t} + \frac{2t\,{\rm e}^{-2k_0t}\beta}{k_0}\Psi_2,$$

$$E = 2k_0\Psi_1,\ \frac{\partial E}{\partial\chi_b} = \frac{\partial k_b}{\partial\chi_b}(\Psi_1+1)+k_0(\Psi_1-1),\ \ F = 2k_0,\ \frac{\partial F}{\partial\chi_b} = \frac{\partial k_b}{\partial\chi_b}(\Psi_1+1)-k_0(\Psi_1-1),$$

$$G = 2k_0\Psi_2,\ \frac{\partial G}{\partial\chi_b} = \frac{\partial k_b}{\partial\chi_b}(\Psi_2+1)+k_0(\Psi_2-1),\ \ H = 2k_0,\ \frac{\partial H}{\partial\chi_b} = \frac{\partial k_b}{\partial\chi_b}(\Psi_2+1)-k_0(\Psi_2-1),$$

$$\frac{\partial k_b}{\partial\chi_b} = \frac{1}{2}\sqrt{k_x^2+\beta^2-\left(\frac{\omega}{c}\right)^2}\,\frac{\beta^2}{k_x^2+\beta^2}.$$

3. Simulation and numerical calculation

As an example, a sheet electron beam interacting with the $\rm TM_{y10}$ mode in the dielectric-loaded RCM is investigated by using the above beam-wave interaction theory. A rectangular waveguide of width 22.86 mm and height 10.16 mm is adopted. The thicknesses of the top and bottom dielectric layer are taken to be 3 mm and 4 mm, respectively. The gap distance between the beam and the bottom dielectric layer is kept unchanged at a value of 0.4 mm. The working frequency, the beam voltage, the current density, and the beam thickness are taken to be 20 GHz, 35 kV, 15 A/cm^2, and 1 mm, respectively.

Figure 2 shows a simulation model of the dielectric-loaded RCM with the input and output tapers of dielectric layer depth. In Fig. 2, the model is divided into five sections, including the input smooth waveguide, the input taper, the dielectric-loaded slow-wave structure, the output taper, and the output smooth waveguide from the left to the right ends. Figure 3 shows the cold dispersion curve of the $\rm TM_{y10}$ mode. Figures 4 and 5 show the field intensity distributions of the electric field component E_z in planes *xoy* and *yoz*, respectively. In Fig. 6, the dotted line corresponds to the result obtained from the ansoft HFSS code, and the dashed line represents the numerical result, where $x = 0$ mm and $z = 20$ mm. The normalized amplitudes of the electric field component E_z of the $\rm TM_{y10}$ mode for $y = -4$ mm and $y = 6.16$ mm approach to zero, which satisfy the boundary conditions of the tangent electric field component, and the amplitude reaches a peak value for $y = -0.4$ mm. Based on the analysis for Figs. 4, 5, and 6, it can be proved that the electromagnetic waves propagate along the surface of the dielectric layer in the RCM. The maximum amplitude of the E_z appears around the dielectric layer surface, and gradually decreases with the increase of distance on the y axis.

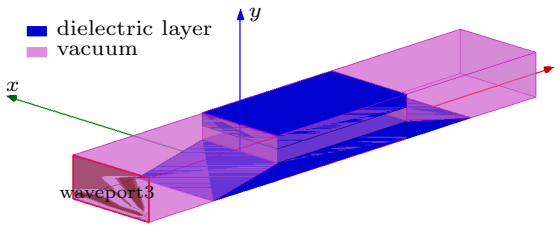


Fig. 2. (colour online) Simulation model of the dielectric-loaded RCM.

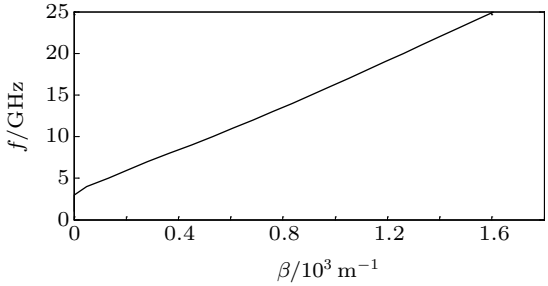


Fig. 3. Cold dispersion curve of the $\rm TM_{y10}$ mode.

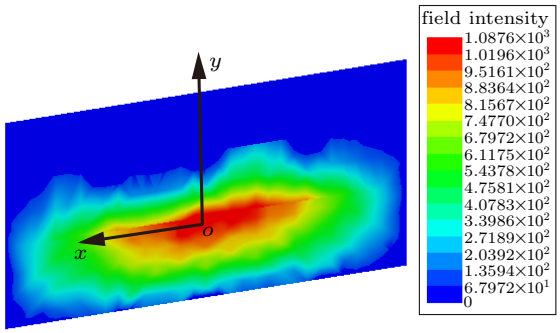


Fig. 4. (colour online) Field intensity distribution of the electric field component E_z in plane xoy.

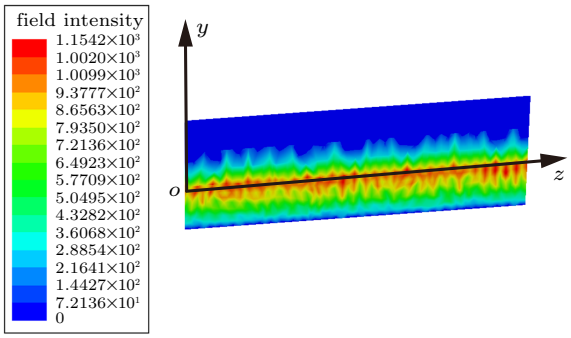


Fig. 5. (colour online) Field intensity distribution of the E_z in plane yoz.

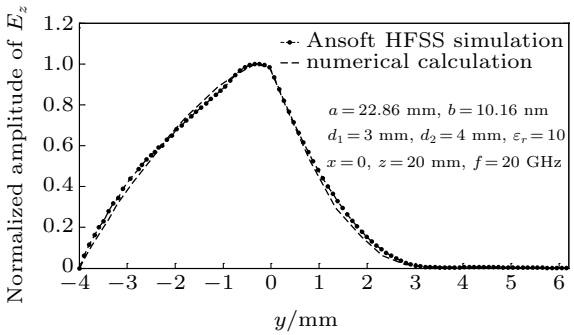


Fig. 6. Normalized amplitude of longitudinal component E_z versus y.

As shown in Fig. 7, the resonant growth rate, G, decreases with the rise of the gap distance between the beam and the bottom dielectric layer, for the beam thickness of 1 mm, the top dielectric-layer thickness of 3 mm and the bottom dielectric-layer thickness of 4 mm. In fact, it is the increase of the gap distance that reduces the coupling between the guided waves and the space-charge waves. In Fig. 8, the gap distance, δ, is kept unchanged at a value of 0.4 mm, the resonant growth rate rises markedly with the increase of beam thickness when the thickness is less than 0.5 mm, this rise slows down when the beam thickness is more than 0.8 mm, and then tends to a saturated value with a further increase of beam thickness. This result shows that the electromagnetic wave energy mainly distributes around the surface of the dielectric layer, and drops quickly with the increase of distance on the y axis. Figure 9 shows that the resonant growth rate rises with the increase of current density, J_b, where the relative dielectric constant ε_r takes a value of 10. Based on the analysis for Figs. 7, 8, and 9, it can be found out that a resonant growth rate of 0.3613 dB/cm is obtained at a working frequency of 20 GHz for a beam voltage of 35 kV and current density of 15 A/cm^2.

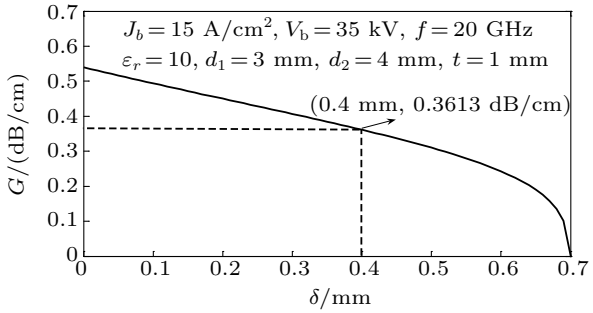


Fig. 7. Resonant growth rate versus the gap distance between the beam and the bottom dielectric layer.

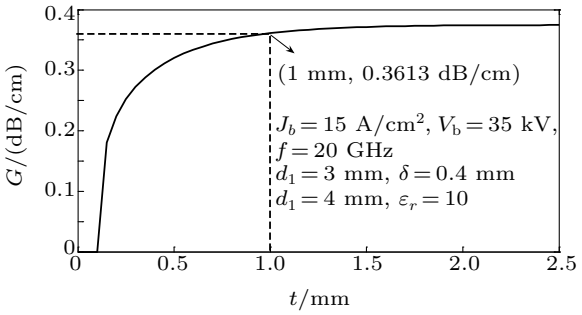


Fig. 8. Resonant growth rate versus beam thickness.

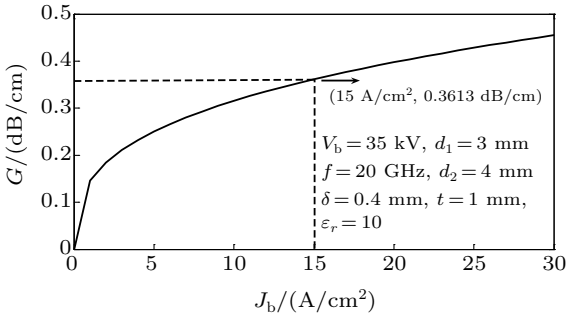


Fig. 9. Resonant growth rate versus current density.

By solving the cold dispersion equation and the 1D space-charge equation, the relationship at the synchronization point between the bottom dielectric layer thickness, d_2, and the beam voltage, V_b, is derived

for the top dielectric-layer thickness, 3 mm. Substituting this relationship into formula (9), the resonant growth rates at different synchronization points can be obtained. Figure 10 denotes that the resonant growth rate increases rapidly with the rise of the beam voltage when the voltage is smaller than 50 kV, this growth slows down when the voltage is larger than 50 kV and approaches to a peak value, and then decreases with the further increase of beam voltage.

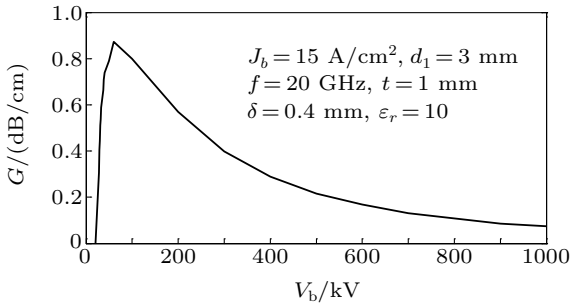


Fig. 10. Resonant growth rate versus beam voltage at synchronization points.

4. Conclusion

A 3D model of the dielectric-loaded RCM for the beam-wave interaction is proposed. The hybrid-mode dispersion equation is obtained by solving the equivalent multi-layer field matching problem. Moreover, the resonant growth rate at the operating point under the assumption of the dilute electron beam is investigated. Through simulation and numerical calculation, the influence of the principal working parameters on the resonant growth rate is analysed. It is worth pointing out that a resonant growth rate of 0.3613 dB/cm can be obtained at a working frequency of 20 GHz for the beam voltage of 35 kV and the current density of 15 A/cm^2.

References

[1] Zhao D, Ding Y, Wang Y and Ruan C 2010 *Phys. Plasmas* **17** 113110

[2] He J, Wei Y Y, Gong Y B, Duan Z Y and Wang W X 2010 *Acta Phys. Sin.* **59** 2843 (in Chinese)

[3] Li Y B, Zhu D J and Liu S G 2008 *Journal of University of Electronic Science and Technology of China* **37** 730 (in Chinese)

[4] Shu W, Wang Y and Zhao D 2011 *High Power Laser and Particle Beams* **23** 1574 (in Chinese)

[5] Dai L 2009 *Ph. D Thesis*, University of Electronic Science and Technology of China (in Chinese)

[6] Walsh J E, Marshall T C and Schlesinger S P 1977 *Phys. Fluids* **20** 709

[7] Felch K L, Busby K O, Layman R W, Kapilow D and Walsh J E 1981 *Appl. Phys. Lett.* **38** 601

[8] Laven S V, Branscum J, Golub J, Layman R and Walsh J E 1982 *Appl. Phys. Lett.* **41** 408

[9] Garate E P, Moustaizis S, Buzzi J M, Rouille C and Lamain H 1986 *Appl. Phys. Lett.* **48** 1326

[10] Kosai H, Garate E, Fisher A and Main W 1992 *IEEE Trans. Plasma Sci.* **20** 288

[11] Shlapakovskii A S 1996 *SPIE* **2843** 137

[12] Walsh J E, Shaughnessy C H, Layman R, Dattoli G, Gallerano G P and Renieri A 1988 *Nucl. Instr. Method* A **272** 132

[13] Garate E, Kosai H, Evans K, Fisher A, Cherry R and Main W 1990 *Appl. Phys. Lett.* **56** 1092

[14] Carlsten B E 2002 *Phys. Plasmas* **9** 1790

[15] Zhang K Q and Li D J 2001 *Electromagnetic Theory for Microwaves and Optoelectronics* (Beijing: Electronics Industry Press) (in Chinese)

[16] Lawson J D 1988 *The Physics of Charged Particles* Chap. 6 (Oxford: Clarendon) p. 293

[17] Joe J, Chang S F, Scharer J and Booske J 1991 *Microwave Opt. Technol. Lett.* **4** 443

[18] Huang H C 1984 *Coupled Mode Theory* (Utrecht: VNU Science Press BV)